Efficient self-cleaning treatments for built heritage based on highly photo-active and well-dispersible TiO_2 nanocrystals

Francesca Gherardi [a,*], Annalisa Colombo [b,c], Massimiliano D'Arienzo [b], Barbara Di Credico [b], Sara Goidanich [a], Franca Morazzoni [b], Roberto Simonutti [b], Lucia Toniolo [a]

[a] Dipartimento di Chimica, Materiali e Ingegneria Chimica "Giulio Natta", Politecnico di Milano, Via Mancinelli 7, 20131 Milan, Italy
[b] Dipartimento di Scienza dei Materiali, Università degli Studi di Milano-Bicocca, Via Roberto Cozzi 55, 20125 Milan, Italy
[c] Fondazione CIFE, Via G. Colombo 81, 20133 Milan, Italy

A B S T R A C T

The present study reports on the preparation and characterization of innovative "self-cleaning" nano-TiO_2 treat-ments to be used in cultural heritage, based on dispersion of solar-light activated TiO_2 nanocrystals. The semicon-ductor has been prepared by an easy and low-cost non-aqueous procedure, providing anatase (NA_TiO_2) nanoparticles photo-active not only under UV-light but also under solar irradiation. NA_TiO_2 allows obtaining very stable dispersions either in water or in ethylene glycol used to produce homogeneous nano-TiO_2 treatments on Noto stone and Carrara marble, which display excellent aesthetic compatibility, do not remarkably affect the capillary water absorption of the stones and slightly increase their wettability.
The new treatment exhibits higher photocatalytic activity compared to that based on commercial TiO_2 (P25_TiO_2). This behavior has been attributed not only to the morphological properties of the treatments and of the stones, but also to the presence of residual benzyl alcohol molecules anchored on the anatase NP surfaces. This provides solar light absorption and partially improves the charge trapping, thus increasing the photoefficiency. The overall results suggest that the positive combination of high dispersion, solar-light absorp-tion and reduced recombination effects in NPs plays a key role in the development of efficient photocatalytic treatments for stone restoration.

Keywords:
Photocatalysis
TiO_2 nanoparticles dispersions
Self-cleaning treatments
Stone

1. Introduction

Environmental pollution due to industrial plants, domestic heating, and transportation is the major responsible for the degradation of historic monuments and buildings in urban areas [1,2]. Therefore, in the last years, many efforts have been devoted to the synthesis of materials able to promote the degradation of environmental contaminants, e.g., by exploiting the well-known photocatalytic properties of different semiconductor metal oxides (e.g., TiO_2, ZnO, WO_3). Among them, TiO_2 is the most widely used because it is inexpensive, safe, chemically stable and displays high photocatalytic efficiency in many procedures (e.g., NO_x, SO_x and VOC abatement, water-cleaning, self-cleaning and antibacterial processes) [3,4]. Under UV irradiation TiO_2 generates electron/hole pairs, which can either recombine or migrate to the material surface where they participate in redox reactions, promoting the removal of organic and inorganic contaminants.

In new building technologies the use of nanostructured TiO_2 based materials as surface coatings, paintings and treatments can provide self-cleaning properties, reducing their maintenance time and cost, preventing the soil accumulation [5,6]. In the conservation of historic buildings and exposed outdoor works of art (e.g., stone monuments, sculptures, fountains), treatments have to respect also some specific requirements such as: chemical inertness, stability, maximum water vapor permeability, no harmful by-products and maintenance of the cultural heritage original aesthetic characteristics [7]. In the literature two categories of self-cleaning treatments for cultural heritage stone surfaces can be identified. The first one comprises nanocomposites where TiO_2, SiO_2, SnO_2 and Al_2O_3 nanoparticles have been introduced inside a polymeric matrix, in order to create nano-roughness on the surfaces and make them hydrophobic and superhydrophobic [8–14]. The second group includes instead hydrophilic photocatalytic TiO_2 nanoparticles (NPs) dispersions, which have been recently applied to different natural stones (limestones, marble, calcarenite, travertine) and renders [15–20]. In these cases, the oxide is used in both amorphous and crystalline phases (i.e., anatase, rutile, brookite or their mixtures) and sometimes

the use of commercial TiO_2-based treatments is reported. Moreover, in order to improve the adhesion of the nanoparticles on the stone surfaces and avoid their release to the environment, an interesting strategy is their incorporation inside a silica matrix which, besides improving the photocatalytic properties, allows an enhancement of the stone strengthening [21–23].

Unfortunately, commercial TiO_2 NPs dispersions present several limitations and stability problems, with agglomeration phenomena; as a consequence, they often give non-homogeneous and whitish films. Moreover, they in general require UV-light activation, showing poor activity under solar irradiation, where the UV component is less than 5%. Within this context, several efforts have been made aiming to modify the structure and the composition of TiO_2 in order to improve the photocatalytic efficiency of these treatments, for instance by increasing the oxide surface area, by harvesting the solar light through doping with transition metal ions (Cr^{3+}, Fe^{3+}) and non-metal atoms (N, S and C) [5,24], or by surface functionalization with suitable organic sensitizers [25,26]. Moreover, noble-metal nanoparticles (gold, silver, platinum) have been used in recent years thanks to their surface plasmon resonance (SPR) phenomenon [27,28].

Nevertheless, the development of solar-light activated treatments containing homogeneously dispersed TiO_2 nanocrystals, which are able to maintain their peculiar photocatalytic properties when deposited on the substrate materials, preserving at the same time the original aesthetic of the surfaces [29] remains an open issue.

Trying to face this challenge, the present study aims at the preparation and characterization of nano-TiO_2 based dispersions used for the development of highly efficient photocatalytic treatments for stone surfaces. A simple and low-cost non-aqueous synthesis in benzyl alcohol has been exploited to obtain anatase (NA_TiO_2) nanoparticles [30], which resulted photo-active not only under UV-light but also under solar irradiation. This additional absorption was attributed to the presence of benzyl alcohol molecules anchored to the surface of the nanocrystals as residuals from the synthesis.

NA_TiO_2 nanoparticles allowed to obtain highly stable dispersions in aqueous systems (water and ethylene glycol), which were then casted on lithotypes with different porosity (Carrara marble and Noto stone). The photocatalytic performances of the obtained nano-TiO_2 treatments have been assessed, paying attention that important requirements, such as the aesthetical compatibility and the main substrates physical properties (water contact angle and capillarity), would be preserved.

The high reactivity of NA_TiO_2 treatment has been finally discussed and related to the electronic structure of the charge trapping centers (Ti^{3+}, O^- and O_2^-), present in irradiated TiO_2 and detected by electron spin resonance (ESR) spectroscopy.

2. Materials and methods

2.1. Preparation of TiO_2 NPs dispersions and their application on stone specimens

TiO_2 nanoparticles (NA_TiO_2) were synthesized according to a non-aqueous synthesis [31], by using benzyl alcohol and titanium (IV) tetrachloride, as solvent and precursor respectively, in agreement with a previous paper [30]. The resulting titania suspension was centrifuged and washed three times, twice with ethanol and once with tetrahydrofuran. The nanoparticles were dried under environmental atmosphere at room temperature overnight and then ground into a powder. The collected powder was weighted and dispersed in the suitable amount of solvent by sonication.

Dispersions of cleaned TiO_2 nanoparticles were prepared by pouring them in water and ethylene glycol using TiO_2 concentrations 1%, 2% and 3% by weight for water (WA) and 1%, 2% and 4% by weight for ethylene glycol (EG). Dispersions have been named WA1, WA2, WA3, EGA1, EGA2 and EGA4. Water and ethylene glycol were selected as solvents because of their different properties in terms of boiling point and volatility.

Water dispersions of commercial TiO_2 nanoparticles AEROXIDE® P25 by Evonik (P25_TiO_2) were also prepared for comparison. According to the literature, these nanoparticles are the most effective commercial ones in terms of photocatalytic activity and they are characterized by the ratio 78:14:8 anatase–rutile–amorphous phase [32,33]. Dispersions were prepared by adding commercial TiO_2 nanoparticles in water with concentrations of 1%, 2% and 3% by weight (labeled as CA1, CA2 and CA3). The nanoparticle size in water and EG dispersions was analyzed by Zetasizer Dynamic Light Scattering (Malvern Instrument Ltd.) at room temperature using a $\lambda = 632.8$ nm He–Ne laser.

Samples of calcarenite (Noto stone) and Carrara marble, having $50 \times 50 \times 10$ mm and $50 \times 50 \times 20$ mm sizes were washed with deionized water and dried at room temperature until a constant mass was achieved (about 2–3 days). Successively, the TiO_2 dispersions were applied on their surfaces by brush. These two lithotypes were selected because of their differences in morphology, especially in terms of open porosity which is around 30% for Noto stone [34] and 2% for Carrara marble [35]. For comparison, untreated stone samples were also studied (named REF).

The loading of titania deposited on each substrate, calculated considering the amount of product required to completely wet the lithotype surface (about 25 cm^2), is reported in Table 1.

2.2. Structural, morphological and optical characterization of TiO_2 nanoparticles

The structural analysis of Aeroxide® P25 and NA_TiO_2 was performed by Powder X-ray diffraction (XRD) using a Bruker D8 DISCOVER with a GADDS microdiffractometer, equipped with a Hi-Star area detector. Nanoparticles size and morphology were studied using transmission electron microscopy (*TEM, Philips CM200-FEG*) operated at 200 kV. Samples of water dispersions were prepared by leaving 1–2 drops onto a carbon coated copper 200 mesh grid. In order to measure the nanoparticle surface area, nitrogen adsorption–desorption isotherms were taken at liquid nitrogen temperature using an ASAP 2010 analyzer (Micrometrics). The powder was outgassed for 12 h at 473 K. The surface area of the nanoparticles was calculated using the Brunauer, Emmet, and Teller model (BET model) [36]. ATR (Attenuated Total Reflectance)-Fourier Transform Infrared (FT-IR) measurements were performed by a Spectrum 100 (Perkin Elmer) spectrophotometer with a resolution of 4 cm^{-1}; 128 scans were acquired. Powder diffuse reflectance spectra were measured by a PerkinElmer Lambda 950 UV–Vis Spectrometer, equipped with an integrating sphere.

2.3. Evaluation of the effectiveness of the nano-TiO_2 treatments applied to stone specimens

Environmental Scanning Electron Microscopy (ESEM) and EDX analyses were performed on the stone surfaces before and after treatments, in order to assess the treatments morphology properties. The penetration depth of TiO_2 nanoparticles into the stone substrate was evaluated by using a Zeiss EVO 50 EP ESEM, equipped with an Oxford INCA 200 — Pentafet LZ4 spectrometer.

The optical properties of the treatments and, in particular, the aesthetical compatibility with the stone were verified by spectrophotometric

Table 1
Average amount of titania deposited on stone samples (mg). The surface area on which the treatments were applied is about 25 cm^2.

	TiO_2 treatments								
	WA1	WA2	WA3	EGA1	EGA2	EGA4	CA1	CA2	CA3
Noto stone	3.5	4.4	9.9	3.4	6.6	9.6	3.4	6.6	9.6
Carrara marble	2.1	4.4	6.0	2.0	4.2	6.9	–	–	–

measurements, carried out directly on the surfaces of three samples per treatment by a Konica Minolta CM-600D instrument, with a D65 illuminant at 8° and wavelength range between 360 nm and 740 nm. Measurements were elaborated according to the CIE L*a*b* standard color system, which describes a color with three different parameters, L*, a*, and b*, measuring respectively brightness, red/green and yellow/blue color intensities. Ten measurements were performed on each area and the average results of L*a*b* were used to calculate the color difference ΔE* between treated and untreated areas:

$$\Delta E* = \left[(L_2 * - L_1*)^2 + (a_2 * - a_1*)^2 + (b_2 * - b_1*)2\right]^{1/2}. \quad (1)$$

This parameter was used to evaluate the aesthetic compatibility of the treatments with the stone surface.

In order to assess the photocatalytic properties of nano-TiO_2 treatments, decomposition tests of an organic colorant (Rhodamine B, rB) were performed. An aqueous solution of rhodamine B (0.05 g/l ± 0.005 g/l) was applied, by using a pipette, to the surface of both untreated and treated samples (1 ml per specimen). Then, after drying in room conditions till constant mass was achieved (about 1–2 days), colorimetric measurements were carried out using a VIS spectrophotometer (Konica Minolta CM-600D instrument, as described above). The degradation of the applied organic dye was monitored by evaluating the color change of the surface exposed in a Suntest CPS$^+$ solar box, equipped with a Xenon arc lamp source and a cut off filter for wavelengths below 290 nm. The used solar radiation used includes UV-B rays which are capable of degrading rB even without photocatalytic nanoparticles. The irradiance was 765 W/m^2 at the same distance (20 cm) for all the samples, at the temperature of 35 °C. The main purpose of this self-cleaning test was the evaluation of nano-TiO_2 treatments photoactivity under solar irradiation. Therefore, in order to better simulate the real conditions of treated and outside exposed stones, a Xenon lamp was used, instead of an UV one, because it emits radiations similar to those of solar light. The colorimetric measurements were performed after 15, 30, 60, 90 and 150 min of irradiation. The chromatic coordinate a* was used to evaluate the photocatalytic discoloration of stain D* over time, by the equation:

$$D* = (|a*(t) - a*(rB)|/|a*(rB) - a*(0)|) * 100 \quad (2)$$

where a*(0) and a*(rB) are the average values of the chromatic coordinate a* before and after the application of the stained solution and a*(t) is the a* value after t hours of light exposure. D* was taken as representative parameter to discriminate the photocatalytic activity of NA_TiO_2 and P25 nano-TiO_2 treatments on the different stone specimens.

To monitor the wettability changes and water absorption of the stone surfaces after the application of the nano-TiO_2 treatments, static contact angle and capillary water absorption test were performed in room conditions, without exposing the samples to solar lamps or UV light. Static contact angle was evaluated on 15 points for each sample (three samples per treatment), according to UNI standard [37], using an OCA (Optical Contact Angle) 20 PLUS (DataPhysics, Germany), with a drop volume of 5 μl, after 10 s. The drop shape was recorded with a camera and the angle between the substrate surface and the tangent from the edge to the contour of the water drop (contact angle) was evaluated. The capillary water absorption of the stone samples was performed according to UNI standard [38] on 50 × 50 × 20 mm samples of Noto stone and Carrara marble before and after the application of the dispersions (three samples per treatment), in room conditions. The test consists in the evaluation of the water absorbed on the sample surface in contact with a bedding layer of filter papers which is saturated with water. The capillary water absorption value per unit area (Q_i, expressed in mg/cm^2) is defined with the expression:

$$Q_i = (m_i - m_0)/A * 1000 \quad (3)$$

where m_i is the mass (g) of the wet sample at time t_i, m_0 is the mass (g) of the dried sample and A is the surface area (cm^2) in contact with the water. The samples were weighed at the following time intervals: 10 min, 20 min, 30 min, 60 min, 4 h, 6 h, 24 h, 48 h. The capillary index (CI) was calculated with the equation:

$$CI = \int_{t_0}^{t_f} (Q_i)dt/Q_{t_f} t_f \quad (4)$$

where $\int_{t_0}^{t_f}(Q_i)dt$ is the area under the absorption curve, Q_{t_f} is the amount of absorbed water per surface unit at the final time t_f. Finally, the absorption coefficient (AC, expressed in mg/(cm^2 s$^{1/2}$)), which is the slope of the straight part of the absorption curve, was calculated from the expression:

$$AC = (Q_{30} - Q_0)/\sqrt{t_{30}} \quad (5)$$

where Q_{30} is the value of the absorbed water per surface unit at 30 min and Q_0 is the intercept of the line in the straight part of the curve. In fact, the trend of the absorption curve is initially linear, with angular coefficient AC, and then a plateau is reached when the sample is saturated with water.

2.4. ESR investigation

The electron spin resonance (ESR) investigation was performed by a Bruker EMX spectrometer working at the X-band frequency and equipped with an Oxford cryostat working in the range of temperature 4–298 K. The powder sample was contained within quartz glass tubes connected both to a high vacuum pumping system and to a controlled gas feed (O_2). Spectra were recorded in vacuum conditions (10^{-5} mbar) at 130 K, before and after 40 min of UV-irradiation at the same temperature inside the EPR cavity. The experimental procedure guaranteed low recombination rate for the photogenerated species. Modulation frequency was 100 kHz, modulation amplitude 2–5 G, and microwave power 10 mW. Irradiation was performed by Vis 150W Xe lamp (Oriel) with the output radiation focused on the samples in the cavity by an optical fiber (50 cm length, 0.8 cm diameter). The *g* values were calculated by standardization with α,α′-diphenyl-β-picryl hydrazyl (DPPH). Care was taken in order to always keep the most sensitive part of the EPR cavity (1 cm length) filled.

3. Results and discussion

3.1. Characterization of synthetized and commercial TiO_2 NPs

Although already described in a previous study [30], the structural, morphological and surface properties of the non-aqueous anatase (NA_TiO_2) sample and of its dispersions were here checked and compared to those of commercial TiO_2 (P25_TiO_2), in order to more easily discuss the photocatalytic properties. Fig. 1a shows the XRD diffraction patterns of P25 and NA_TiO_2 nanopowders. The diffraction pattern for the commercial product confirmed the presence of a mixture of anatase–rutile–amorphous phases with a ratio of 78:14:8. The exclusive presence of anatase was instead detected in NA_TiO_2 nanoparticles (Fig. 1b). The average crystallite size has been evaluated from the (101) peak for anatase (peak "A") and from the (110) peak for rutile (peak "R"), by using the Scherrer equation. For P25, the average anatase and rutile nanoparticle dimensions were 24 and 31 nm, respectively. The average crystallite size for anatase TiO_2 resulted ~5.6 nm.

Nitrogen physisorption experiments were performed on both NA_TiO_2 and P25 nanocrystals. Samples are mesoporous and show a type IV Brunauer isotherm. As an example, the adsorption–desorption isotherms and the corresponding monomodal pore-size distribution of NA_TiO_2 nanoparticles are shown in Fig. S1 (Appendix A). According to the t-plot, no micropores were detected. The specific surface area

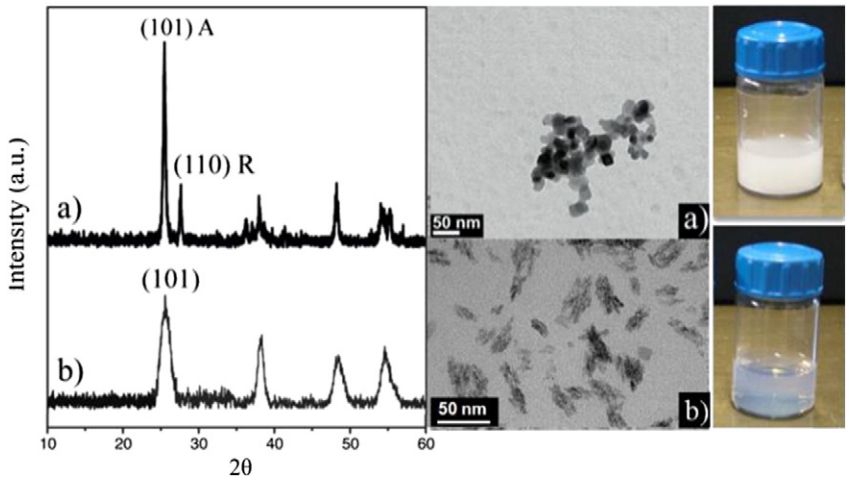

Fig. 1. XRD patterns and TEM micrographs of titanium dioxide nanoparticles: a) P25_TiO_2 b) NA_TiO_2. On the right, the pictures of the respective TiO_2 dispersions in water (1% by weight).

(SSA_{BET}) of anatase resulted 249 m^2/g, while P25 nanocrystals displayed significantly lower SSA_{BET} (50 m^2/g).

XRD and BET results are in good agreement with TEM images reported in Fig. 1. In fact, NA_TiO_2 nanoparticles appear almost spherical with a size of about 5–6 nm, aggregated in elongated structures whose longest axis measures about 40 nm. P25 nanocrystals are instead clustered in oversize and misshapen structures.

The possibility to obtain a stable dispersion of titania nanoparticles in water and EG was investigated by DLS measurements. In particular, once dispersed in water and EG, NA_TiO_2 presents a hydrodynamic diameter of 40 ± 20 nm, without any further larger aggregate, in reasonable agreement with the TEM images. Instead, it was impossible to obtain a DLS value for P25 nanoparticles, since the nanopowder precipitates within few minutes. This result agrees with the presence of big aggregates in P25, and reveals a difficulty to disperse these nanoparticles in highly polar environments, despite the hydrophilic surface. The different optical behaviors of the two dispersions can be assessed by simple visual inspection of the pictures reported in Fig. 1. In fact, while the P25_TiO_2 dispersion in water appears white and opaque, due to the light scattering (Mie diffusion) of nanoparticle aggregates, NA_TiO_2 dispersion is essentially transparent and shows like a blue-sky effect, attributable to Rayleigh scattering. This suggests that nanoparticles have a size of about one order of magnitude less than the visible light wavelengths.

The surface structure of both types of nanopowders was investigated by ATR-FTIR spectroscopy (Fig. 2). The only vibrational modes detectable in the P25_TiO_2 spectrum (see Fig. 2a) are the O–H stretching and bending vibrations (at about 3380 cm^{-1} and 1628 cm^{-1}, respectively), due to water physisorbed on the titanium dioxide surface. Instead, the IR spectrum of NA_TiO_2 (see Fig. 2b) shows a very strong intensity band and a frequency shift of the O–H stretching from 3380 cm^{-1} to 3145 cm^{-1}, attributable to chemisorbed hydroxyl groups covalently bonded to the oxide. Moreover, weak peaks at ~1500 cm^{-1} related to species chemisorbed on the surface become clearly visible. These are probably attributable to benzyl alcohol residues, due to the absorptions of the aromatic C–H groups (see magnification of the spectra in Fig. 2).

Diffuse UV–visible reflectance spectra have been recorded and converted into absorption spectra by the Kubelka–Munk procedure. Fig. 3 shows that in the case of NA_TiO_2 powder an absorption is detectable in the visible frequency region, instead the P25_TiO_2 reflectance spectrum in the same region is flat. The difference can be related to the presence of benzyl alcohol bound to the surface of NA_TiO_2. This generates defects within the TiO_2 energy gap due to the mixing of oxide orbitals with those of the anchored alcohol group, and allows the red-shift of the NA_TiO_2 absorption edge [39].

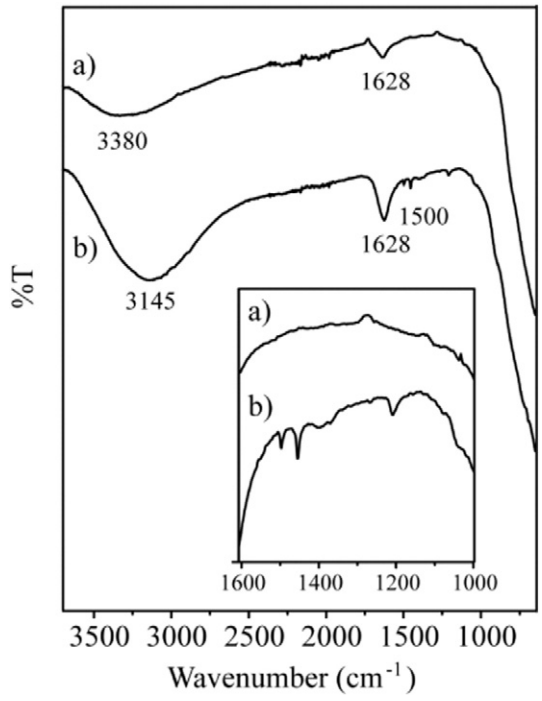

Fig. 2. Comparison between FTIR spectra of P25_TiO_2 (a) and NA_TiO_2 (b) nanoparticles. Inset: the magnification of the 1600–1000 cm^{-1} region.

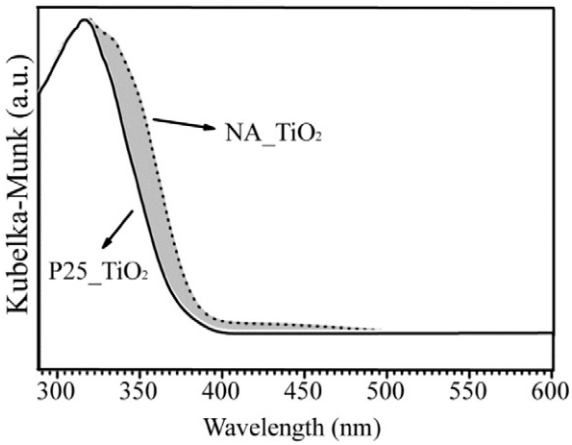

Fig. 3. UV–visible spectra of P25_TiO_2 and NA_TiO_2 nano-powders.

These results are in agreement with a previous study, where the presence of residual benzyl alcohol molecules strongly interacting with the anatase surface has been proved by ^{1}H Magic Angle Spinning (MAS) NMR measurements [30].

3.2. Evaluation of the effectiveness of nano-TiO_2 treatments

3.2.1. Morphology of the treated surfaces and penetration depth of nano-TiO_2 treatments

In order to better compare the efficacy of the different nano-TiO_2 treatments, Table 1 reports the amount of titania (mg) deposited on the stone specimens. It can be observed that Noto stone, due to its larger porosity, requires a higher amount of dispersed matter than Carrara marble to treat the same surface area. As a consequence, the absolute amount of TiO_2 deposited on Noto stone is higher than on Carrara marble, even if the effective residual remained at the surface is lower, due to the penetration of the nanoparticles into the pores (see Aesthetic compatibility section) [34,35].

SEM–EDX analyses were performed on untreated and treated samples of Carrara marble and Noto stone with the aim of studying the morphology and the penetration depth of the nano-TiO_2 treatments. In particular, the results obtained from specimens treated with the nanodispersion having the highest NA_TiO_2 loading either in water (WA3) or in ethylene glycol (EGA4) are reported (Fig. 4), together with those of specimens treated with the dispersion containing the lowest loading of P25_TiO_2 nanoparticles (CA1). CA2 and CA3 showed whitening effects on the stone surfaces (see next section). Since the samples treated with WA1, WA2, EGA1 and EGA2 do not show any relevant differences in terms of morphology compared to the samples treated with WA3 and EGA4, the corresponding images were not shown.

Both NA_TiO_2 derived from the dispersions in water and ethylene glycol and P25_TiO_2 are not homogeneously distributed on the surface of Noto stone specimens (Fig. 4a, c, e). This is probably related to the high porosity of the stone, which does not allow the creation of continuous films for both the dispersions, leading to aggregation of titania nanoparticles mostly inside

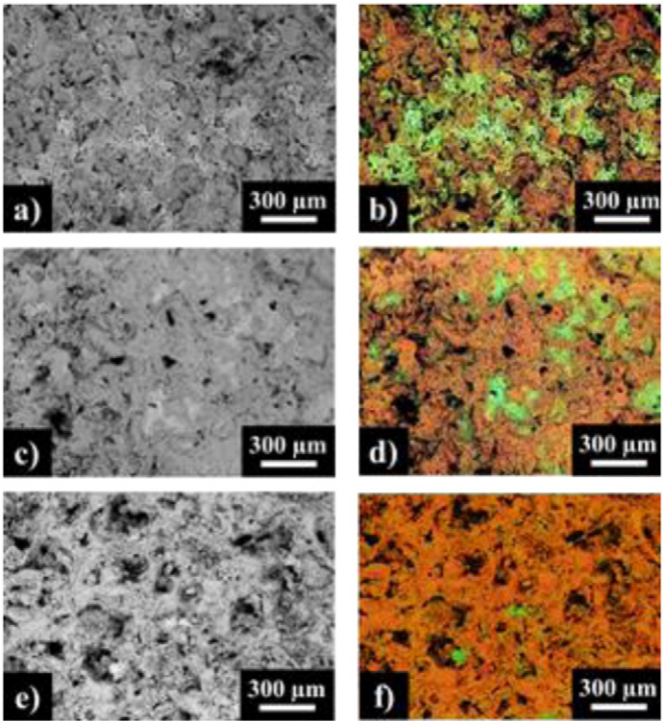

Fig. 4. ESEM–EDX characterization of the Noto stone surface treated with WA3 (a), EGA4 (c) and CA1 (e) dispersions. False color images indicate the corresponding distribution of titanium (green) and calcium (orange) (b, d, and f).

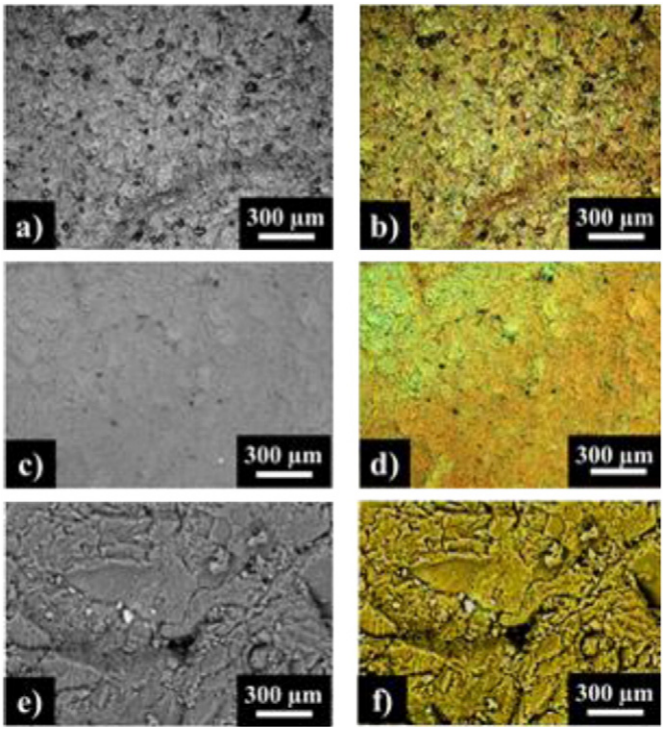

Fig. 5. ESEM–EDX characterization of the Carrara marble surface treated with WA3 (a), EGA4 (c) and CA1 (e), and the corresponding false color images indicating the distribution of titanium (green) and calcium (orange) (b, d and f).

pores, even in depth. As shown in false color images (Fig. 4b, d, f), nanoparticles are more finely dispersed in substrates treated with NA_TiO_2 compared to those treated with P25_TiO_2. This suggests a poorer adhesion of the commercial treatment on the stone surface.

On Carrara marble specimens (Fig. 5), NA_TiO_2 treatments (in WA and EG) created instead a continuous film on the surface with no cracks (Fig. 5a and c), whereas with commercial dispersion aggregation of nanoparticles occurs (Fig. 5e). The corresponding false color images are reported in Fig. 5b, d, and f.

By observing the sections, in Noto stone specimens, TiO_2 nanoparticles reach a penetration depth of about 300–500 μm (Fig. 6a), because of

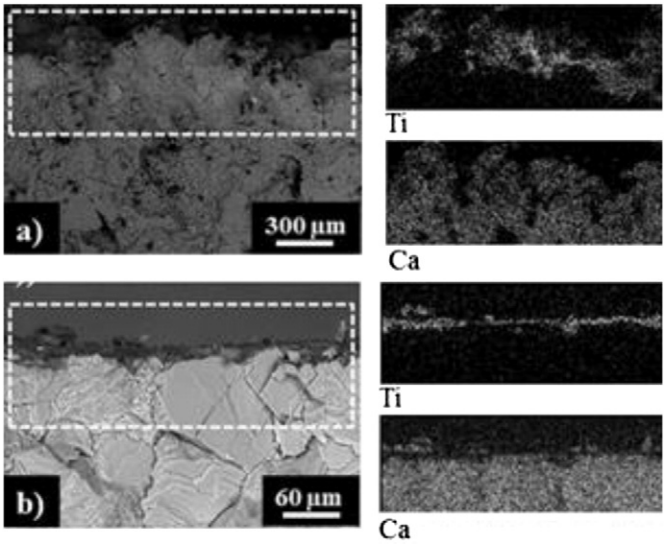

Fig. 6. ESEM–EDX characterization of the section of Noto stone (a) and Carrara marble (b) samples treated with EGA4 and distribution of calcium and titanium.

Table 2
ΔE* values of Noto stone and Carrara marble surface specimens before and after the application of nano-TiO_2 treatments.

	ΔE*								
	WA1	WA2	WA3	EGA1	EGA2	EGA4	CA1	CA2	CA3
Noto stone	0.12 ± 0.08	0.40 ± 0.12	0.16 ± 0.01	0.22 ± 0.02	0.33 ± 0.12	0.69 ± 0.56	3.60 ± 1.40	8.73 ± 3.49	8.91 ± 3.61
Carrara marble	1.02 ± 0.51	1.35 ± 0.91	1.19 ± 0.64	1.23 ± 0.28	1.12 ± 0.18	0.83 ± 0.39	1.27 ± 0.65	5.45 ± 0.91	5.89 ± 1.15

the stone porosity, thus reducing the amount of photocatalytic titania on the surface. On the other hand, on Carrara marble specimens, the nano-TiO_2 treatments cover mainly the surface and penetrate only within few microns (Fig. 6b).

3.2.2. Aesthetic compatibility

Color measurements were performed on the surface of the stone specimens before and after the application of the nano-TiO_2 treatments, in order to verify the preservation of their original aesthetic appearance. Table 2 shows the results of the colorimetric tests in terms of ΔE* values for each treatment and for both the stone substrates (Noto stone and Carrara marble). The application of the NA_TiO_2 dispersions (WA1, WA2, WA3, EGA1, EGA2, EGA4) does not produce any relevant modification (see Table 2). Conversely, water dispersions containing commercial TiO_2 in amount >1% (CA2, CA3) cause the whitening of the stone surfaces, leading to ΔE* values higher than 5. This is the maximum value of ΔE* acceptable for restoration treatments in the frame of cultural heritage [40]. For this reason, CA2 and CA3 dispersions have been discarded for both lithotypes while only the CA1 with P25_TiO_2 with 1% by weight was considered acceptable for comparison with the other samples. As Table 2 shows, ΔE* values of Noto stone specimens treated with NA_TiO_2 dispersions are lower compared to those obtained from Carrara marble specimens, probably due to the penetration of the dispersions inside the pores of the substrates, although the amount of products applied on Noto stone is higher (see Table 1).

3.2.3. Evaluation of photocatalytic activity

Fig. 7 reports the trend of rhodamine B discoloration along the time, after pre-fixed intervals of exposition to Xenon lamp irradiation, of stone specimens either untreated (Reference, REF) or treated with NA_TiO_2 treatments (WA1, WA2, WA3, EGA1, EGA2, EGA4) and with commercial titania treatments (CA1). Table 3 reports the ratios between the stain discoloration D* values for Noto stone and Carrara marble specimens treated with the highest concentration of NA_TiO_2 in ethylene glycol (EGA4) and 1% TiO_2_P25 (CA1) and of the reference sample (REF).

For both Noto stone and Carrara marble specimens, the best performances in terms of photocatalysis are achieved by the treatment with the highest nano-TiO_2 concentration (EGA4), whereas the use of a specific solvent does not seem to be a discriminating factor.

For Noto stone samples (Fig. 7a), the D* values progressively increase during the UV–Vis irradiation and reach a plateau after a reaction time of 80 min, probably due to the slowing of the degradation kinetics. As shown in Table 3 and in Fig. 7, at the end of the test the photocatalytic activity of the specimens treated with NA_TiO_2 is always higher than that of the sample coated with P25_TiO_2 and of the reference. In particularly, D^*_{EGA4}/D^*_{REF} is 1.59 while D^*_{CA1}/D^*_{REF} is 1.20.

This indicates that the presence of NA_TiO_2 treatments promotes a more efficient degradation and the fading of the red colorant over long periods.

In the case of Carrara marble samples, a sharp increase of the D* can be observed within the first minutes of the reaction and, for the specimens treated with NA_TiO_2, the plateau is reached just after 20 min of UV–Vis irradiation (Fig. 7b). As observed for Noto stone, the photoactivities of the samples treated with NA_TiO_2 treatments are higher than those of CA1 and the reference (Table 3), confirming the suitability of the NA_TiO_2 NPs for the development of efficient treatments in stone restoration. In particular, at the end of the test D^*_{EGA4}/D^*_{REF} is 1.29 and D^*_{CA1}/D^*_{REF} is 1.03, indicating a similar behavior of the specimen treated with CA1 compared to the reference.

Further, it can be noticed a faster degradation of the colorant on Marble samples compared to Noto stone. As an example, EGA4 treatment on marble specimens leads to the 70% of discoloration in the first 15 min (Fig. 7b), while in the case of Noto stone the same nano-TiO_2 treatments give rise only to the 38% of discoloration in the same time frame (Fig. 7a). Moreover, for this latter lithotype, the highest D* values are achieved with the highest NA_TiO_2 concentrations (WA3 and EGA4) after 100 min of irradiation. Conversely, for Carrara marble the best photocatalytic activity is reached by nano-TiO_2 treatments containing the highest NA_TiO_2 concentration in EG (EGA4) after about 60 min.

These results can be ascribed to the higher open porosity of Noto stone (about 30%) [34] compared to Carrara marble (about 2%) [35], which induces a significant TiO_2 NPs penetration into the bulk (see Section 3.2.1), thus decreasing the amount of photocatalytic titania at the surface and leading to lower activity.

3.2.4. Wettability and water absorption properties

Static contact angle measurements were performed on marble specimens to evaluate the wettability change of the stone surfaces after the application of NPs dispersions. For the Noto stone, the contact angle test could not be performed, because of the intrinsic high porosity; in fact the water drop was lost (absorbed) within the first 10 s. The values of static contact angles of treated and untreated Carrara marble specimens

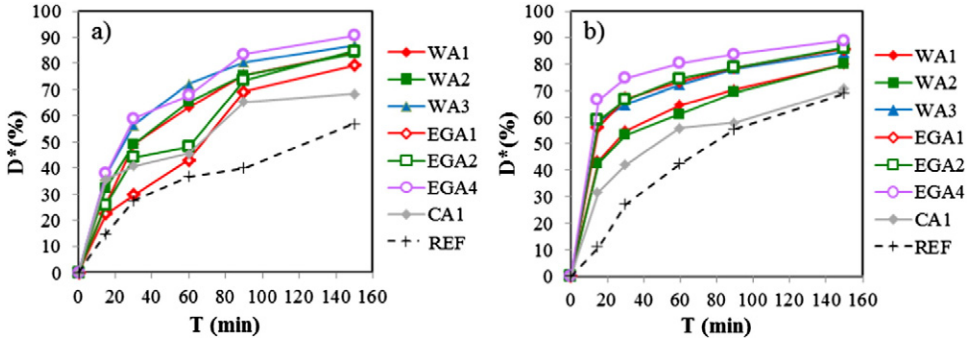

Fig. 7. Stain discoloration values D* (%) as a function of time (min) for Noto stone (a) and Carrara marble (b) after pre-fixed intervals of irradiation in solar box.

Table 3
Ratio between the values of stain discoloration D* of samples treated with EGA4 (D^*_{EGA4}) and CA1 (D^*_{CA1}) and the reference (D^*_{REF}) for Noto stone and Carrara marble samples.

	Noto stone		Carrara marble	
Time (min)	D^*_{EGA4}/D^*_{REF}	D^*_{CA1}/D^*_{REF}	D^*_{EGA4}/D^*_{REF}	D^*_{CA1}/D^*_{REF}
15	2.57	2.42	6.10	2.91
30	2.14	1.48	2.76	1.55
60	1.85	1.24	1.90	1.32
90	2.09	1.63	1.51	1.04
150	1.59	1.20	1.29	1.03

are presented in the diagram of Fig. 8. Two reference samples were prepared; the first one is an untreated sample (REF), the second one (REF_EG) is a sample previously treated with ethylene glycol, helpful to compare the contact angle value with that of samples treated with nano-TiO_2 dispersions in ethylene glycol. Compared to stones treated with WA1, WA2 and WA3, those treated with EG1, EG2 and EG4 show higher contact angles, even for reference samples (REF and REF_EG). This suggests that ethylene glycol lowers the wettability of stone surfaces. However, θ values of samples treated with both water and ethylene glycol dispersions (WA and EG) are lower than those of the reference samples (REF and REF_EG respectively). This means that the treatment with NA_TiO_2 changes the marble wettability and induces modifications that make the stone surfaces more hydrophilic than the reference ones [41]. This behavior is attributable to the *superhydrophilic effect*, which is even more favored by the light absorption in the visible region and by the high dispersion of NA_TiO_2.

The treatment with P25_TiO_2 does not modify the surface wettability of the stones, due to the fact that P25 requires UV-irradiation for photoexcitation and to the evidence of nanoparticle aggregation [42].

The results of capillary water absorption tests for Noto stone and Carrara marble samples are shown in Fig. 9, with the graphs of Q_i values as a function of square root of time ($t_i^{1/2}$). In Noto stone (Fig. 9a, b), there are no significant differences between the curves measured before and after the application of nano-TiO_2 dispersions and the Qi values result very high, according to the enhanced porosity of the lithotype. This behavior should be ascribed to the intrinsic inhomogeneities of samples in terms of porosity and roughness. Instead, for Carrara marble specimens (Fig. 9c, d), Q_i values are lower, due to the high density of the substrate, and remarkably changes after the application of nano-TiO_2 dispersions in ethylene glycol. In particular, it can be observed that EGA4 treatment does not alter the capillary water absorption while, unexpectedly, EGA1 and EGA2 proportionally modify it. However, water absorption on marble is very low and these differences are meaningful only from a proportional point of view. The values of the maximum water absorption (Q_i), capillarity index (CI) and absorption coefficient before (nt.) and after (t.) the application of the treatments are summarized in Table S1 (see Supporting Information). The results of untreated and treated samples

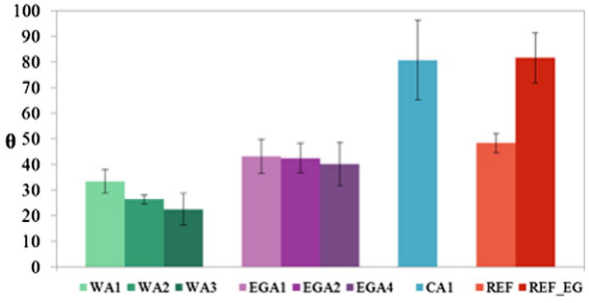

Fig. 8. Contact angle values of Carrara marble samples, treated with new synthetized titania treatment (WA1, WA2, WA3, EGA1, EGA2, EGA4), with commercial titania (CA1), untreated reference (REF) and reference treated with ethylene glycol (REF_EG).

are very similar and only those of samples treated with EGA1, EGA2 and EGA4 differ.

3.3. ESR investigation

In order to go deeper insight into the high photocatalytic activity of NA_TiO_2, a comprehensive EPR investigation on the formation and the reactivity of the charge trapping centers formed upon UV–Vis irradiation, was performed.

After irradiation in vacuum (Fig. 10a), samples show two well separated sets of resonance lines. The lower field weak resonances with $g_\perp = 2.0126$ and $g_\parallel = 2.0046$, having nearly axial symmetry, are characteristic of holes trapped at O^- centers [43]. The intense and broad feature arising in the spectrum at higher magnetic field is instead attributable to the superimposition of different Ti^{3+} species (electron traps): the narrow signal (A) at $g_{A\perp} = 1.985$ corresponds to the perpendicular *g*-tensor component of the anatase Ti^{3+} lattice centers ($g_{A\parallel}$ is not detectable due to overlap with the other lines); the two broad signals (B and C) may be associated to electrons trapped on two others distinct surface Ti^{3+} centers located at the surface ($g_B = 1.934$, and $g_C = 1.954$).

These results can be discussed in terms of crystal field around a metal ion with d^1 electronic configuration, lying in a tetragonally distorted octahedral geometry. The *g* values depend on the extent of tetragonal distortion and are reproduced by the following expressions:

$$g_\parallel = 2 - 8\lambda/\Delta\Delta = E(d_{x2-y2}) - E(d_{xy}) \quad (6)$$

$$g_\perp = 2 - 2\lambda/\delta\delta = E(d_{xz,yz}) - E(d_{x2-y2}) \quad (7)$$

where Δ and δ are the energy differences between the orbitals interacting through spin orbit coupling and λ is the spin-orbit coupling constant. Thus, increasing the value of the tetragonal distortion, the $g_\perp$ value increases approaching 2.

In the present case, while the coordination environment of lattice Ti^{3+} centers (A) keeps always the same, that of surface Ti^{3+} centers (B and C) undergoes changes. Coherently, we observed for these surface traps an increase of $g_\perp$ value compared to that reported for surface Ti^{3+} species, usually $g = 1.926$ [44]. This shift is more significant for the C species, indicating a larger tetragonal distortion than for the B one. In accordance with IR and NMR results, we suggest that one or more benzyl alcohol molecules are coordinated to B and C Ti^{3+} centers, modifying the crystal field parameters owing to the covalent contribution of the sigma interaction [44]. The number of coordinated alcohol molecules is probably different between B and C species and higher for C.

Interestingly, it can be observed that the amount of photogenerated electron traps (Ti^{3+}) is very high in NA_TiO_2, if compared to the quantity of O^- species (trapped holes). A similar behavior has been already reported for UV-irradiated colloidal TiO_2 systems in the presence of methanol. In detail, it has been suggested that the addition of methanol, which is an effective hole scavenger, results in the formation of the electron-donating species $\bullet CH_2OH$ ($E^\circ(\bullet CH_2OH/CH_2O) = -0.95$ V) which induces an electron injection into colloidal TiO_2 with formation of additional surface electron traps and formaldehyde. The net result is that from the absorption of one photon of light two electrons are injected, and this phenomenon is known in electrochemistry as a *current-doubling effect* [45].

An analogous mechanism may be invoked for the NA_TiO_2, where benzyl alcohol is covalently interacting with surface Ti ions. As suggested by Feng et al. [46], during UV-irradiation, the benzyl alcohol molecules react with photogenerated holes producing benzyl alcohol radicals, which may inject electrons to TiO_2 and provide extra surface Ti^{3+} traps. This effect may further enhance the photoefficiency of NA_TiO_2 treatments.

In order to further investigate the nature and the role of these Ti^{3+} species in the photocatalytic process, EPR spectra on NA_TiO_2 were

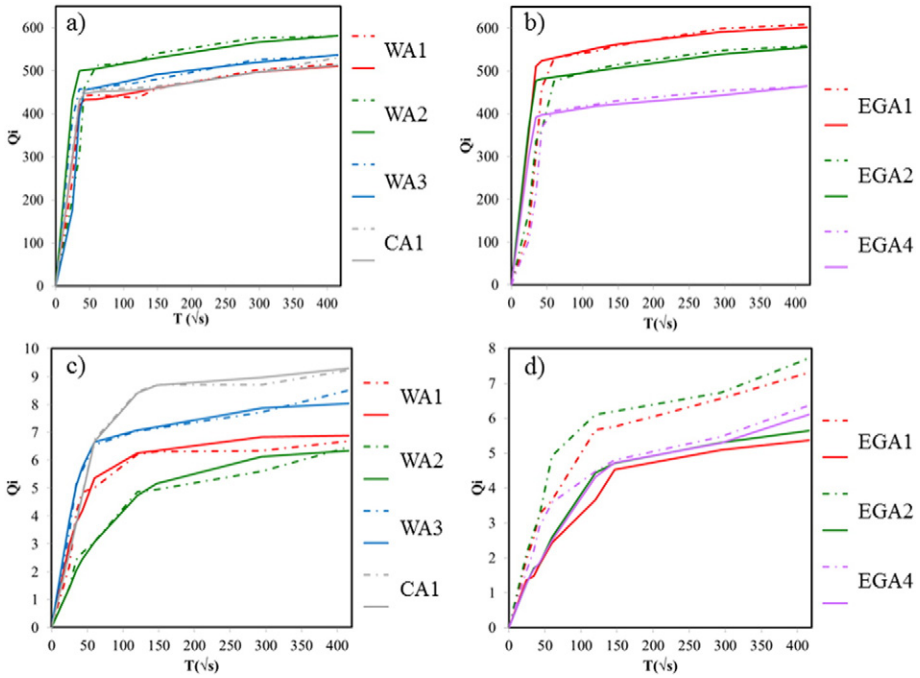

Fig. 9. Graphs of water absorption by capillarity before (dashed lines) and after (solid lines) the application of the titania water and ethylene glycol dispersions on Noto stone (a and b) and on Carrara marble (c and d).

performed after UV–Vis irradiation at 130 K in the presence of $p(O_2) = 10$ mbar and subsequent evacuation at $p < 10^{-5}$ mbar.

The resonances of Ti^{3+} and of O_2^- centers ($g_{zz} = 2.0290$, $g_{yy} = 2.0086$, $g_{xx} = 1.9990$) can be easily detected (Fig. 10b). The intensity of the B and C signals becomes much lower than that detected in vacuo, while that of bulk Ti^{3+} centers (A) remains more-less constant. This on one hand confirms the surface location of these species and on the other one indicates an enhanced reactivity of these surface traps, which in principle are able to give, by electron transfer, Ti^{4+}–O_2^- species active in the photooxidative processes.

These results again support the good photoactivity of NA_TiO_2 treatments under UV–Vis light.

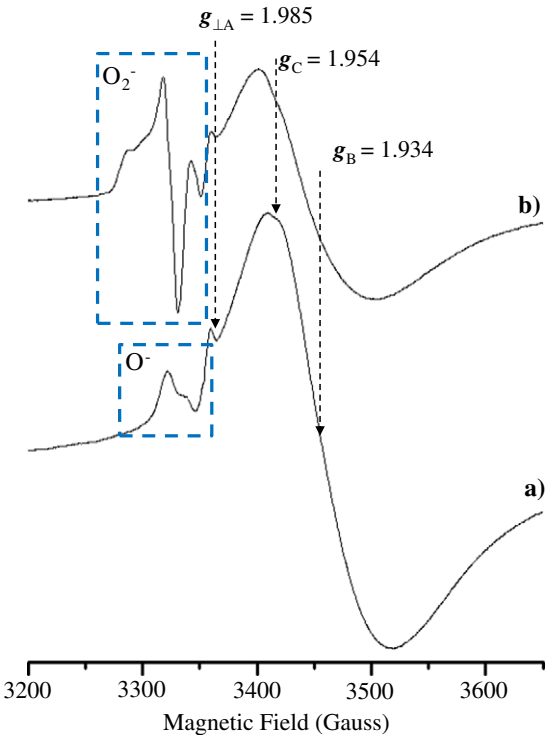

Fig. 10. EPR spectra at 130 K of NA_TiO_2 after UV–Vis irradiation a) in vacuum ($p < 10^{-5}$ mbar) and b) in the presence of $p(O_2) = 10$ mbar.

4. Conclusions

The present study describes the preparation and the characterization of nano-TiO_2 based dispersions (NA_TiO_2), used for the development of novel highly photocatalytic treatments for a good maintenance and conservation of stone surfaces.

The dispersions are aqueous-based (water and ethylene glycol are used as solvents), respecting the important requirements of safety and green chemistry, and highly stable, avoiding problems of precipitation and – as a consequence – reliability. Moreover, they are cheap and simple to be used by spraying or brushing according to the substrate needs.

The NA_TiO_2 treatments, obtained by brushing the dispersions on stone surfaces, showed better aesthetical compatibility compared to that made with commercial TiO_2 (P25_TiO_2).

The improvement above described has been connected both to the morphological properties of the nano-TiO_2 treatments and to the different porosity of the lithotypes.

In detail, ESEM–EDX revealed that the NA_TiO_2 treatments are highly homogeneous on marble, preserving both the nanoparticles active surface area and the optical quality of the stone substrate. Instead, in Noto stone samples, NA_TiO_2 treatments do not create continuous films but lead to nanoparticles aggregation into the pores, thus reducing the photoactivity of the stone samples. For both lithotypes, P25_TiO_2 dispersions provided inadequate treatments from either morphological or optical points of view, due to significant nanoparticles aggregation and agglomeration on the stone surface.

The solar light absorption also improves the charge trapping supplying additional surface electron traps (Ti^{3+} centers), thus increasing the photoefficiency of NA_TiO_2 treatments regardless of the nature of the stone substrates.

The overall results suggest that the positive combination of high NPs dispersion, solar-light absorption and higher amount of surface electron

trap offers an important chance for the development of highly efficient photocatalytic treatments for stone conservation.

Appendix A. Supplementary Data

Supplementary data to this article can be found online at http://dx.doi.org/10.1016/j.microc.2015.11.043.

References

[1] G.G. Amoroso, V. Fassina, Stone Decay and Conservation: Atmospheric Pollution, Cleaning, Consolidation, and Protection Amsterdam; New York1983.
[2] A. Bonazza, C. Sabbioni, N. Ghedini, Quantitative data on carbon fractions in interpretation of black crusts and soiling on European built heritage, Atmos. Environ. 39 (2005) 2607–2618.
[3] X. Chen, S.S. Mao, Titanium dioxide nanomaterials: synthesis, properties, modifications, and applications, Chem. Rev. 107 (2007) 2891–2959.
[4] J. Zhao, X. Yang, Photocatalytic oxidation for indoor air purification: a literature review, Build. Environ. 38 (2003) 645–654.
[5] A. Fujishima, X. Zhang, Titanium dioxide photocatalysis: present situation and future approaches, C. R. Chim. 9 (2006) 750–760.
[6] J. Chen, C.-s. Poon, Photocatalytic construction and building materials: from fundamentals to applications, Build. Environ. 44 (2009) 1899–1906.
[7] E.F. Doehne, C.A. Price, Stone Conservation: An Overview of Current Research. , Getty Conservation Institute, Los Angeles, 2010.
[8] G. Cappelletti, P. Fermo, M. Camiloni, Smart hybrid coatings for natural stones conservation, Progress in Organic Coatings
[9] C. Kapridaki, P. Maravelaki-Kalaitzaki, TiO_2–SiO_2–PDMS nano-composite hydrophobic coating with self-cleaning properties for marble protection, Prog. Org. Coat. 76 (2013) 400–410.
[10] C. Kapridaki, L. Pinho, M.J. Mosquera, P. Maravelaki-Kalaitzaki, Producing photoactive, transparent and hydrophobic SiO_2-crystalline TiO_2 nanocomposites at ambient conditions with application as self-cleaning coatings, Appl. Catal. B Environ. 156–157 (2014) 416–427.
[11] M.F. La Russa, S.A. Ruffolo, N. Rovella, C.M. Belfiore, A.M. Palermo, M.T. Guzzi, G.M. Crisci, Multifunctional TiO_2 coatings for cultural heritage, Prog. Org. Coat. 74 (2012) 186–191.
[12] P.N. Manoudis, I. Karapanagiotis, A. Tsakalof, I. Zuburtikudis, B. Kolinkeová, C. Panayiotou, Superhydrophobic films for the protection of outdoor cultural heritage assets, Appl. Phys. A 97 (2009) 351–360.
[13] P.N. Manoudis, A. Tsakalof, I. Karapanagiotis, I. Zuburtikudis, C. Panayiotou, Fabrication of super-hydrophobic surfaces for enhanced stone protection, Surf. Coat. Technol. 203 (2009) 1322–1328.
[14] D. Colangiuli, A. Calia, N. Bianco, Novel multifunctional coatings with photocatalytic and hydrophobic properties for the preservation of the stone building heritage, Constr. Build. Mater. 93 (2015) 189–196.
[15] L. Bergamonti, I. Alfieri, A. Lorenzi, A. Montenero, G. Predieri, G. Barone, P. Mazzoleni, S. Pasquale, P.P. Lottici, Nanocrystalline TiO_2 by sol–gel: characterisation and photocatalytic activity on Modica and Comiso stones, Appl. Surf. Sci. 282 (2013) 165–173.
[16] E. Franzoni, A. Fregni, R. Gabrielli, G. Graziani, E. Sassoni, Compatibility of photocatalytic TiO_2-based finishing for renders in architectural restoration: a preliminary study, Build. Environ. 80 (2014) 125–135.
[17] L. Luvidi, G. Laguzzi, F. Gallese, A.M. Mecchi, G. Sidoti, Application of TiO_2 based coatings on stone surfaces of interest in the field of cultural heritage, in: G.E. srl (Ed.), 4th International Congress on Science and Technology for the Safeguard of Cultural Heritage in the Mediterranean Basin, A. Ferrari, Il Cairo 2010, pp. 495–500.
[18] A. Licciulli, A. Calia, M. Lettieri, D. Diso, M. Masieri, S. Franza, R. Amadelli, G. Casarano, Photocatalytic TiO_2 coatings on limestone, J. Sol-Gel Sci. Technol. 60 (2011) 437–444.
[19] I. Poulios, P. Spathis, A. Grigoriadou, K. Delidou, P. Tsoumparis, Protection of marbles against corrosion and microbial corrosion with TiO_2 coatings, J. Environ. Sci. Health A 34 (1999) 1455–1471.
[20] E. Quagliarini, F. Bondioli, G.B. Goffredo, C. Cordoni, P. Munafò, Self-cleaning and depolluting stone surfaces: TiO_2 nanoparticles for limestone, Constr. Build. Mater. 37 (2012) 51–57.
[21] L. Pinho, F. Elhaddad, D.S. Facio, M.J. Mosquera, A novel TiO_2–SiO_2 nanocomposite converts a very friable stone into a self-cleaning building material, Appl. Surf. Sci. 275 (2013) 389–396.
[22] L. Pinho, M.J. Mosquera, Titania–silica nanocomposite photocatalysts with application in stone self-cleaning, J. Phys. Chem. C 115 (2011) 22851–22862.
[23] L. Pinho, M.J. Mosquera, Photocatalytic activity of TiO_2–SiO_2 nanocomposites applied to buildings: influence of particle size and loading, Appl. Catal. B Environ. 134–135 (2013) 205–221.
[24] I.P. Parkin, R.G. Palgrave, Self-cleaning coatings, J. Mater. Chem. 15 (2005) 1689–1695.
[25] J. Schneider, M. Matsuoka, M. Takeuchi, J. Zhang, Y. Horiuchi, M. Anpo, D.W. Bahnemann, Understanding TiO_2 photocatalysis: mechanisms and materials, Chem. Rev. 114 (2014) 9919–9986.
[26] D. Duonghong, E. Borgarello, M. Grätzel, Dynamics of light-induced water cleavage in colloidal systems, J. Am. Chem. Soc. 103 (1981) 4685–4690.
[27] L. Chen, S. Yang, B. Hao, J. Ruan, P.-C. Ma, Preparation of fiber-based plasmonic photocatalyst and its photocatalytic performance under the visible light, Appl. Catal. B Environ. 166–167 (2015) 287–294.
[28] L. Pinho, M. Rojas, M.J. Mosquera, Ag–SiO_2–TiO_2 nanocomposite coatings with enhanced photoactivity for self-cleaning application on building materials, Appl. Catal. B Environ. 178 (2015) 144–154.
[29] L. Bergamonti, I. Alfieri, M. Franzò, A. Lorenzi, A. Montenero, G. Predieri, M. Raganato, A. Calia, L. Lazzarini, D. Bersani, P. Lottici, Synthesis and characterization of nanocrystalline TiO_2 with application as photoactive coating on stones, Environ. Sci. Pollut. Res. (2013) 1–14.
[30] A. Colombo, F. Tassone, M. Mauri, D. Salerno, J.K. Delaney, M.R. Palmer, R.D.L. Rie, R. Simonutti, Highly transparent nanocomposite films from water-based poly(2-ethyl-2-oxazoline)/TiO_2 dispersions, RSC Adv. 2 (2012) 6628–6636.
[31] M. Niederberger, M.H. Bartl, G.D. Stucky, Benzyl alcohol and titanium tetrachloride – a versatile reaction system for the nonaqueous and low-temperature preparation of crystalline and luminescent titania nanoparticles, Chem. Mater. 14 (2002) 4364–4370.
[32] T. Ohno, K. Sarukawa, K. Tokieda, M. Matsumura, Morphology of a TiO_2 photocatalyst (Degussa, P-25) consisting of anatase and rutile crystalline phases, J. Catal. 203 (2001) 82–86.
[33] B. Ohtani, O.O. Prieto-Mahaney, D. Li, R. Abe, What is Degussa (Evonik) P25? Crystalline composition analysis, reconstruction from isolated pure particles and photocatalytic activity test, J. Photochem. Photobiol. A Chem. 216 (2010) 179–182.
[34] L. Anania, A. Badalà, G. Barone, C.M. Belfiore, C. Calabrò, M.F. La Russa, P. Mazzoleni, A. Pezzino, The stones in monumental masonry buildings of the "Val di Noto" area: new data on the relationships between petrographic characters and physical–mechanical properties, Constr. Build. Mater. 33 (2012) 122–132.
[35] T. Poli, L. Toniolo, O. Chiantore, The protection of different Italian marbles with two partially fluorinated acrylic copolymers, Appl. Phys. A 79 (2004) 347–351.
[36] S. Brunauer, P.H. Emmett, E. Teller, Adsorption of gases in multimolecular layers, J. Am. Chem. Soc. 60 (1938) 309–319.
[37] E.C.f. Standardization, Conservation of Cultural Property – Test Methods – Determination of Static Contact Angle2009.
[38] E.C.f. Standardization, Conservation of Cultural Property – Test Methods – Determination of Water Absorption by Capillarity2009.
[39] R. Li, H. Kobayashi, J. Guo, J. Fan, Visible-light induced high-yielding benzyl alcohol-to-benzaldehyde transformation over mesoporous crystalline TiO_2: a self-adjustable photo-oxidation system with controllable hole-generation, J. Phys. Chem. C 115 (2011) 23408–23416.
[40] O. García, K. Malaga, Definition of the procedure to determine the suitability and durability of an anti-graffiti product for application on cultural heritage porous materials, J. Cult. Herit. 13 (2012) 77–82.
[41] R. Wang, K. Hashimoto, A. Fujishima, M. Chikuni, E. Kojima, A. Kitamura, M. Shimohigoshi, T. Watanabe, Light-induced amphiphilic surfaces, Nature 388 (1997) 431–432.
[42] S. Banerjee, D.D. Dionysiou, S.C. Pillai, Self-cleaning applications of TiO_2 by photo-induced hydrophilicity and photocatalysis, Appl. Catal. B Environ. 176–177 (2015) 396–428.
[43] R. Scotti, M. D'Arienzo, A. Testino, F. Morazzoni, Photocatalytic mineralization of phenol catalyzed by pure and mixed phase hydrothermal titanium dioxide, Appl. Catal. B Environ. 88 (2009) 497–504.
[44] T. Rajh, A.E. Ostafin, O.I. Micic, D.M. Tiède, M.C. Thurnauer, Surface modification of small particle tich colloids with cysteine for enhanced photochemical reduction: an EPR study, J. Phys. Chem. 100 (1996) 4538–4545.
[45] G. Nogami, J.H. Kennedy, Investigation of 'current doubling' mechanism of organic compounds by the rotating ring disk electrode technique, J. Electrochem. Soc. 136 (1989) 2583–2588.
[46] W. Feng, G. Wu, L. Li, N. Guan, Solvent-free selective photocatalytic oxidation of benzyl alcohol over modified TiO_2, Green Chem. 13 (2011) 3265–3272.